International Journal of Solids and Structures 71 (2015) 194–205

Contents lists available at ScienceDirect

International Journal of Solids and Structures

journal homepage: www.elsevier.com/locate/ijsolstr

Pattern transformation of thermo-responsive shape memory polymer periodic cellular structures

Yuhao He [a], Siusiu Guo [a], Zishun Liu [a,*], K.M. Liew [b]

[a] International Center for Applied Mechanics, State Key Laboratory for Strength and Vibration of Mechanical Structures, Xi'an Jiaotong University, Xi'an 710049, China
[b] Department of Architecture and Civil Engineering, City University of Hong Kong, Tat Chee Avenue, Kowloon, Hong Kong

ARTICLE INFO

Article history:
Received 17 February 2015
Received in revised form 18 June 2015
Available online 29 June 2015

Keywords:
Generalized Maxwell model
Pattern transformation
Periodic cellular structures
Shape memory polymers
Thermo-mechanical viscoelasticity

ABSTRACT

In this paper, pattern transformation behaviors of shape memory polymer (SMP) periodic cellular structures are investigated through numerical simulations. In order to describe SMP cellular structures behavior in the shape memory cycle, generalized thermo-mechanical viscoelasticity theory coupling time–temperature effect are utilized with the generalized Maxwell model and the Williams–Landel–Ferry (WLF) equation. Similar to other normal periodic cellular structures, SMP periodic cellular structures also display the interesting phenomenon of novel pattern transformation when the structures are loaded by compression force beyond a critical value. Different from other periodic cellular materials, novel transformed pattern for SMP material can be fixed via cooling to a temperature below the glass transition temperature T_g, and this fixed pattern can further be recovered to its original pattern by reheating to a temperature above T_g. Moreover, viscous property of SMP during shape memory cycle is taken into account by considering the effects of nominal strain rate and temperature on the pattern transformation. Time–temperature superposition principle is adopted to explain these effects. On the other hand, this transformation phenomenon for SMP can be triggered even by the stress relaxation process. It is also observed that the auxetic behavior (negative Poisson ratio) exists in the pattern transformation during both the compression process and the stress relaxation process for SMP periodic cellular structures. With present study, we are able to gain deeper insights and explain some of the new interesting physical phenomena observed in reported experiments for SMP periodic cellular structures. Besides, these new findings can be used to design appropriate SMP structures in special applications.

1. Introduction

Shape memory polymers (SMPs) are polymeric smart materials that have the ability to fix a deformed state (temporary shape) and to recover back to their original states (permanent shapes) upon the application of certain external stimuli. These external stimuli include heat, pH, magnetic field, light and so on (Behl et al., 2013; Lendlein et al., 2005; Liu et al., 2007). Over the past decade, SMPs have been investigated intensively by many researchers, as they possess a number of advantages over other shape memory materials, including large recoverable strain (reported at over 400% in comparison with 8% for Ni-Ti SMA), low energy consumption for shape programming, light weight, low cost, excellent manufacturability and bio-degradability (Chen and Lagoudas, 2008a,b; Lendlein and Kelch, 2002; Liu et al., 2006; Mather et al., 2009; Morshedian et al., 2005; Qi et al., 2008; Qiao et al., 2013; Tobushi et al., 1997, 2001). Because of these excellent advantages, SMPs have been widely applied as microsystem actuator components, biomedical devices, aerospace deployable structures and morphing structures in the aerospace industry and biomedical engineering (Liu et al., 2004; Tobushi et al., 1996; Yakacki et al., 2007).

Shape recovery triggered by temperature change is known as the thermally induced shape memory effect. Fig. 1 shows a typical SMP deformation circle for thermally induced shape memory material. In step 1, named the loading step, the SMP is pre-deformed from an initial shape (permanent state A) to a deformed shape (temporary state B1) by applying a mechanical load at the higher temperature T_h. The corresponding strain and stress at state B1 are denoted as pre-strain and pre-stress states. Followed by step 2, named the cooling process, it will maintain the pre-deformed shape until the temperature arrives at the lower temperature T_l (temporary state B2). Subsequent to this is step 3, named the unloading process (from temporary state B2 to temporary state B3), where the externally applied loading is removed at

* Corresponding author.
E-mail address: zishunliu@mail.xjtu.edu.cn (Z. Liu).

http://dx.doi.org/10.1016/j.ijsolstr.2015.06.022
0020-7683/

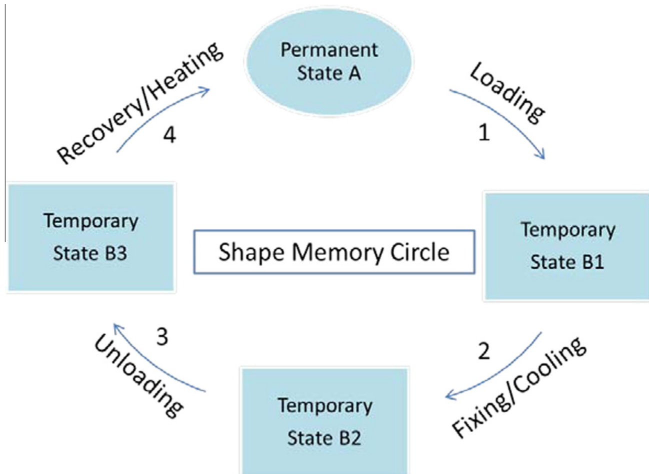

Fig. 1. Typical shape memory circle.

the lower temperature T_l. Finally, in step 4 (from temporary state B3 to permanent state A), this shape memory effect is activated by increasing the temperature again, whereupon the initial shape is recovered to permanent state A.

To study SMP's deformation behaviors and shape memory cycle, different constitutive models have been developed to characterize the complex thermo-mechanical properties of SMPs in the last few years. Most of the earlier theories adopted rheological models and their constitutive models usually consist of simple elements such as spring, dashpot and slip (frictional) elements (Abrahamson et al., 2003; Bhattacharyya and Tobushi, 2000; Lin and Chen, 1999; Morshedian et al., 2005; Tobushi et al., 1997, 2001). These models are capable of capturing the characteristics of the shape memory behavior of SMPs and usually give predictions that are only qualitatively agreed with experimental results. Later developed models are often divided into two general categories: micro modeling and macro modeling (Baghani et al., 2013; Chen and Lagoudas, 2008a,b; Diani and Gall, 2007; Liu et al., 2006; Nguyen et al., 2008; Qi et al., 2008). The micro models are useful for understanding the fundamental molecular mechanism but they are not easily applicable at the structural scale (Nguyen et al., 2010; Xu and Li, 2010). On the other hand, macro models are appropriate for studying deformation and shape memory mechanisms at the structural level and are easily realized with numerical methods such as finite element commercial software, but they can only phenomenologically describe the material behavior. Among these models, the generalized Maxwell model proposed by Diani et al. is more popular and can be easily adopted (Diani et al., 2012). In this model, the time–temperature dependence of the viscoelastic properties of the SMPs was determined using a dynamic mechanical analysis procedure of relatively small-strain large-deformation torsion tests (Diani et al., 2011); no other experiments or fitting parameters were needed. Implementation of the model in numerical analysis was based only on a combination of standard features from commercially available finite element codes and did not call for the contribution of any additional elaborate complex routines. Although the model is simple, it is capable not only of reproducing the experimental shape memory tests precisely and accurately, but also of predicting the shape memory response of thermally activated SMPs with varying compositions, structures and geometries under varying thermo-mechanical conditions. Arrieta et al. have carried out experiments and validated that the Diani et al. model can be applied to large uniaxial strain and shape memory composites (Arrieta et al., 2014a,b). Since this model has these advantages and the viscoelastic theory of the generalized Maxwell model can be realized easily in the commercial finite element package of ABAQUS, we will use the generalized Maxwell model proposed by Diani et al. (2012) to carry out our simulations.

The periodic cellular structures come from the natural world, such as iridescent phenomena in butterflies, beetles, moths, birds and fish (Prum et al., 2006; Vukusic and Sambles, 2003). The novel pattern transformation appears when the periodic cellular structure is compressed beyond a critical value. In the pattern transformation, switching to a new configuration is normally caused by local elastic instabilities, and it is often reversible and repeatable (Mullin et al., 2007). There are many factors that affect the pattern transformation of periodic cellular structures, such as the initial porosity of the structures (Bertoldi et al., 2010), the arrangement of the holes (Bertoldi and Boyce, 2008), the loading case (Michel et al., 2007), the shape of the holes (Hu et al., 2013) and the inclusions in the holes (Hu et al., 2014; Mullin et al., 2013). While these types of cellular structures have been widely investigated in relation to their special mechanical properties of novel pattern transformation, the mechanical behavior of SMP periodic cellular structures, where the material of periodic cellular structures involves smart material with shape memory effects, has not been investigated in detail. Although Mullin et al. referred to the pattern transformation of SMP periodic cellular structures induced by compression, they did not provide complete investigation process details for the shape memory behaviors and failed to consider the effect of the viscosity of materials (Mullin et al., 2007). In the present study, we will intensively study the deformation behaviors of SMP periodic cellular structures with typical shape memory behaviors. Based on experimental observations and understandings of the underlying physical mechanism of shape memory behavior, a generalized Maxwell model is adopted to describe the viscoelastic thermo-mechanical response of materials. The Williams–Landel–Ferry (WLF) equation is adopted to capture time–temperature dependent behaviors. In our study, pattern transformations caused by compression and stress relaxation are considered in the shape memory circle. The effects of temperature and loading speed on pattern transformation are taken into account and the mechanism of pattern transformation is explained using the time–temperature superposition principle. With some examples, it is demonstrated that the viscoelastic theory of the generalized Maxwell model can be easily implemented in finite element simulations, and that the present numerical simulation model is efficient in verifying the thermo-mechanical experiments of Diani et al. (2012).

The article is organized as follows. In Section 2, we introduce the viscoelastic theory of the generalized Maxwell model and the corresponding material parameters used in the present study. Then, we utilize the proposed model to simulate the pattern transformations of the SMP material periodic cellular structures. The simulations include two cases, one is the pattern transformation during uniaxial compression and the other is the pattern transformation during stress relaxation. Finally, we present summary and concluding remarks.

2. Viscoelastic theory

Based on the theory proposed by Diani et al. (2012), we have adopted the generalized finite deformation viscoelasticity theory (Simo, 1987) coupling with the time–temperature effect of amorphous networks, i.e., the generalized Maxwell model (also known as the Maxwell–Weichert model, as shown in Fig. 2) and coupling with the WLF equation to describe the viscoelastic behavior of the amorphous polymer (epoxy 12DA3) utilized in the present study.

To calculate the finite strain behavior, we adopt the finite strain viscoelasticity theory. Here neo-hookean model is employed to describe the hyperelastic behavior as follows,

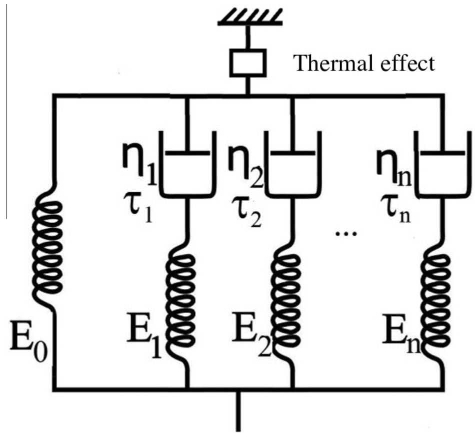

Fig. 2. Generalized Maxwell model.

$$U = C_{10}(\bar{I}_1 - 3) + \frac{1}{D_1}(J_{el} - 1)^2 \tag{1}$$

where $C_{10} = G_0/2$, $D_1 = 2/K_0$, G_0 and K_0 are the initial shear modulus and bulk modulus, $\bar{I}_1$ is the first strain invariant, J_{el} is the elastic volume strain,

$$J_{el} = \frac{J}{J_{th}} \tag{2}$$

where J is the total volume strain and J_{th} is the thermal volume strain,

$$J_{th} = (1 + \varepsilon_{th})^3 \tag{3}$$

where ε_{th} is the linear thermal expansion strain.

In order to take into account of viscoelastic property for SMP material, the basic hereditary integral formulation for linear isotropic viscoelasticity is

$$\boldsymbol{\sigma}(t) = \int_0^t 2G(\tau - \tau')\dot{\mathbf{e}}dt' + \mathbf{I}\int_0^t K(\tau - \tau')\dot{\phi}dt' \tag{4}$$

where $\boldsymbol{\sigma}$ is the instantaneous Cauchy stress, $\mathbf{e}$ and ϕ are the mechanical deviatoric and volumetric strains, '·' denotes differentiation with respect to t', K and G are the time-dependent small-strain shear and bulk relaxation moduli, which are functions of the reduced time τ,

Using integration by parts and a variable transformation, Eq. (4) can be written in the form as follows,

$$\boldsymbol{\sigma}(t) = 2G_0\mathbf{e}(t) + \int_0^\tau 2\dot{G}(\tau')\mathbf{e}(t - t')d\tau' + \mathbf{I}(K_0\phi(t) + \int_0^\tau \dot{K}(\tau')\phi(t - t')d\tau') \tag{5}$$

where G_0 and K_0 are the instantaneous small strain shear and bulk moduli. $\dot{G}(\tau') = dG(\tau')/d\tau'$, and $\dot{K}(\tau') = dK(\tau')/d\tau'$. For the non-isothermal process, recall that the reduced time τ represents a shift in time with temperature

$$\frac{d\tau}{dt} = \frac{1}{a_T(T(t))} \tag{6}$$

where $a_T(T)$ is the time–temperature superposition shifting factor following the classic Williams–Landel–Ferry (WLF) equation,

$$\lg(a_T) = \frac{-C_1(T - T_{ref})}{C_2 + T - T_{ref}} \tag{7}$$

where C_1 and C_2 are material constants. T_{ref} is the WLF reference temperature. According to Diani et al., the parameters are taken as $C_1 = 10.17$, $C_2 = 47.35$ °C, $T_{ref} = 50$ °C.

In constitutive Eq. (5), the relaxation moduli $G(t)$ and $K(t)$ are expressed in terms of Prony series to implement the viscoelasticity theory in ABAQUS,

$$G(\tau) = G_\infty + \sum_{i=1}^{n_G} G_i e^{-\tau/\tau_i^G}, \quad K(\tau) = K_\infty + \sum_{i=1}^{n_K} K_i e^{-\tau/\tau_i^K} \tag{8}$$

where G_∞ and K_∞ represent the shear and bulk moduli at time $t = \infty$. In general, the number of terms in bulk and shear moduli, n_K and n_G, need not be equal to each other, and in many practical cases it can be assumed that $n_K = 0$. Additionally, it is assumed that $n_G = n$ and $\tau_i = \tau_i^K = \tau_i^G$. In order to be consistent with the data from DMA experiments, the moduli are alternated to another form in the frequency domain using Fourier transformations. Both the shear and bulk moduli can be divided into two parts, the storage modulus and the loss modulus.

$$G_s(\omega) = G_0 + \sum_{i=1}^{n} \frac{G_i\tau_i^2\omega^2}{1 + \tau_i^2\omega^2}, \quad G_l(\omega) = \sum_{i=1}^{n} \frac{G_i\tau_i\omega}{1 + \tau_i^2\omega^2} \tag{9}$$

$$K_s = K_0, \quad K_l = 0 \tag{10}$$

where subscript s is the storage modulus, subscript l is the loss modulus and ω is the sweep frequency. The bulk modulus is taken as a constant value $K_0 = 3.1$ GPa in the present study. With experimental DMA data in Diani et al. (2011,2012) and using a time–temperature superposition principle, the storage modulus in the frequency domain was expressed as follows:

$$G_s(\omega) = G_e + \sum_{i=1}^{12} \frac{G_i\tau_i^2\omega^2}{1 + \tau_i^2\omega^2} \tag{11}$$

where $G_e = 1.6$ MPa, and τ_i and G_i ($i = 1, 2, \ldots, 12$) are series of relaxation times and relaxation moduli respectively; their values are listed in Table 1.

To consider the effect of thermal expansion, the coefficients of linear thermal expansion are taken as 5.7×10^{-5} °C^{-1} in the glassy state and 2.44×10^{-6} °C^{-1} in the rubbery state.

The viscoelastic theory of the generalized Maxwell model described above can be realized easily in the commercial finite element package of ABAQUS (Appendix Ashows ABAQUS input file), and all the parameters can be derived and obtained from the work of Diani et al. (2012).

3. Pattern transformation

To study the pattern transformation of SMP periodic cellular structures, the finite element package of ABAQUS is used to carry out the simulations. In the simulations, the constitutive model used to describe SMP behaviors is the generalized Maxwell model, which considers the viscosity of material. Two types of pattern transformations are investigated in the following: one is induced by compression load and the other is induced by stress relaxation.

3.1. Pattern transformation induced by compression

Novel pattern transformation triggered by reversible elastic instability under uniaxial compression in periodic cellular structures has been investigated by many researchers (Bertoldi et al., 2010; Hu et al., 2013; Mullin et al., 2007; Willshaw and Mullin, 2012). In our previous study, we have studied the effect of the hole's shape (Hu et al., 2013) and inclusions (Hu et al., 2014) on the pattern transformation. However, there was little consideration for SMP periodic cellular structures even though they possess many unique mechanical properties. In our present study, we investigate the pattern transformation of SMP periodic cellular structures.

Table 1
Generalized Maxwell model relaxation times and associated shear moduli pairs (Diani et al., 2012).

τ_i (s)	0.3031×10^{-4}	0.1721×10^{-3}	0.9768×10^{-3}	0.5545×10^{-2}	0.3147×10^{-1}	0.1787
G_i (Pa)	0.1476×10^{9}	0.1756×10^{9}	0.2025×10^{9}	0.1775×10^{9}	0.6802×10^{8}	0.1139×10^{8}
τ_i (s)	0.1014×10^{1}	0.5757×10^{1}	0.3268×10^{2}	0.1855×10^{3}	0.1053×10^{4}	0.5977×10^{4}
G_i (Pa)	0.2264×10^{7}	0.8132×10^{6}	0.4020×10^{6}	0.1760×10^{6}	0.5056×10^{5}	0.1265×10^{5}

First, we investigate the critical porosity for SMP cellular structures, which is a prerequisite for pattern transformation. It is noted that the temperature effect is governed by the time–temperature superposition theory stated in the following discussion, thus we do only the test at a higher temperature in order to save time. A number of simulation tests of SMP with different porosities have been carried out. Finally, we found that the critical porosity is about 0.18 for SMP case, which is lower than 0.34 in Bertoldi's case (Bertoldi et al., 2010). This difference may likely be caused by the viscoelastic property of SMP.

In the simulations, we consider a representative volume element (RVE) with appropriate periodic boundary conditions to eliminate boundary condition effects. The RVE model is a $40 \times 40 \times 2\ \text{mm}^3$ plate sample (plain strain or plain stress cases) with periodic circle holes, as shown in Fig. 3. The diameters of the circle holes are 8.67 mm, which gives a porosity of 0.59 larger than the critical porosity.

Then, we reproduce our previous work using a type of hyperelastic material named PSM-4 with this RVE model, and the model is applied with a uniaxial compression as shown in Fig. 3. Assuming the length changes induced by compression are ΔL_1 and ΔL_2 respectively, the nominal strain can be defined as $-\Delta L_1/L_1$ and the nominal transverse strain can be defined as $\Delta L_2/L_2$. Thus, the Poisson ratio is defined as the ratio of nominal transverse strain and nominal strain,

$$v = -\frac{\Delta L_2/L_2}{\Delta L_1/L_1} \tag{12}$$

The nominal stress versus nominal strain curve and the Poisson ratio versus nominal strain curve are shown in Fig. 4. When the model is compressed beyond a critical value, the gradual and homogeneous compression of the periodic cellular hole pattern is replaced by a transformation to a totally different pattern of alternating mutually orthogonal ellipses. After pattern transformation, the cellular structures display new properties; for example, the initial linear elastic behavior is replaced by a plateau stress, and negative Poisson ratio appears. As shown in Fig. 4, the curves depart from their initial behavior at a nominal strain value of about 0.035, which corresponds to pattern transformation. The nominal strain value is known as the critical nominal strain, and the nominal stress at the critical nominal strain is known as the critical nominal stress.

For SMP material, we use the same geometrical model for modeling the periodic cellular structures. The simulation processes of shape memory circles, as illustrated in Fig. 5, are expressed as follows: ① pre-deformation: at the high temperature (70 °C, above T_g), the lower end of the model is fixed with the displacement of the y-direction while the upper end of the model for Fig. 5(a) (or the platen for Fig. 5(b)) is applied with a uniaxial compression at a constant nominal strain rate of 0.01 s^{-1} to a nominal strain of 0.1; ② strain storage: keep the nominal strain constant for Fig. 5(a) (or maintain the position of the platen for Fig. 5(b)) and cool the sample to the low temperature (0 °C, below T_g) at a temperature rate of 14 °C/min; ③ low temperature unloading: release the nominal strain constraint for Fig. 5(a) (or remove the platen for Fig. 5(b) in the simulation only the contact between the platen and the sample is removed) in 1 s at the low temperature and maintain the low temperature for another 99 s; ④ free strain recovery: reheat the sample to the initial high temperature (70 °C) at a temperature rate of 14 °C/min.

Normally there are two types of loading cases for periodic cellular structures. For the loading case as shown in Fig. 5(a), four cycle steps are used. In the first step, during the loading process at high temperature, the pattern transformation occurs at a nominal strain value of about 0.049, while the nominal stress decreases after the transformation and quickly reaches a plateau stress at the zooming part, as shown in Fig. 6. In the second step, the strain is kept constant and the compressive nominal stress decreases as the temperature decreases due to thermal contraction. When the compressive nominal stress decreases to zero, it changes to tensile nominal stress and the tensile nominal stress increases as the temperature decreases. In the third step, the strain constraint is removed in the glassy state. Due to the higher elastic modulus at lower temperatures, the nominal strain recovery is very low compared to the pre-deformation nominal strain. After unloading, no recovery strain appears during the following 99 s at 0 °C; that is to say, the deformation is fixed during the second step. In the fourth step, during the reheating process, the deformation is fully recovered to its initial state.

The loading case shown in Fig. 5(b) is the same as the loading case of Fig. 5(a) in the first step. However, in the second step, no tensile nominal stress appears after the compressive nominal stress decreases to zero. Instead, the nominal stress remains at zero, the sample continues to contract and the sample is separated

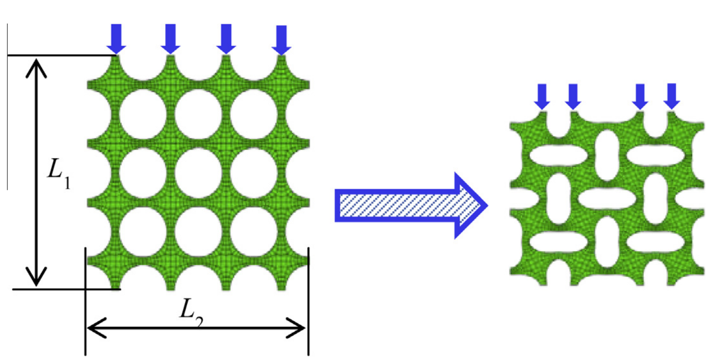

Fig. 3. Schematic plot for pattern transformation induced by compression.

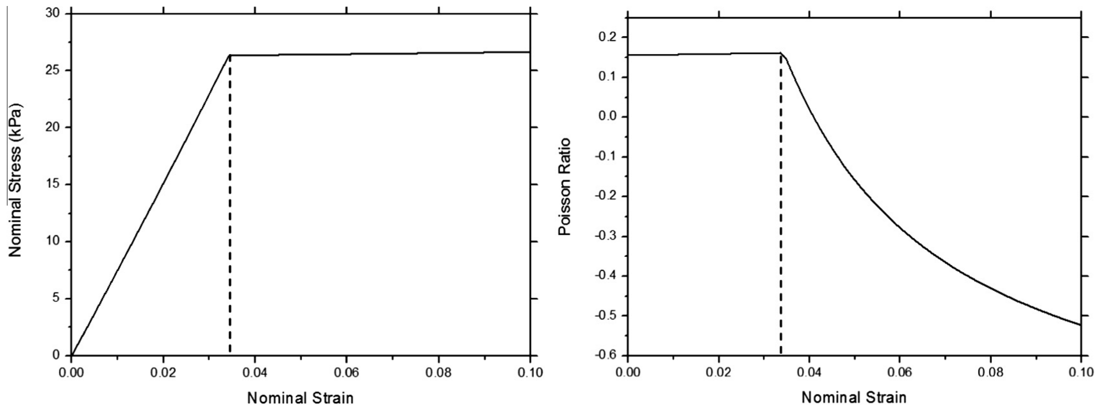

Fig. 4. Nominal stress versus nominal strain curve and Poisson ratio versus nominal strain curve of periodic cellular structures with circle holes and porosity of 0.59.

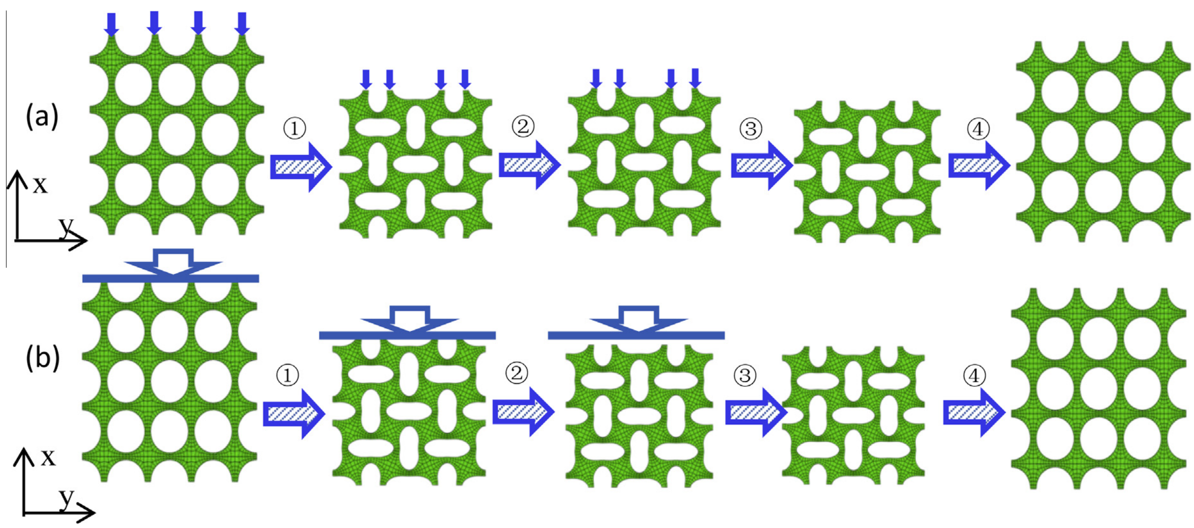

Fig. 5. Schematic plot of loading cases: (a) the compressive load is exerted to the upper surface of the sample; (b) the compressive load is exerted with a platen. ①–④ represent the four steps in the shape memory circle.

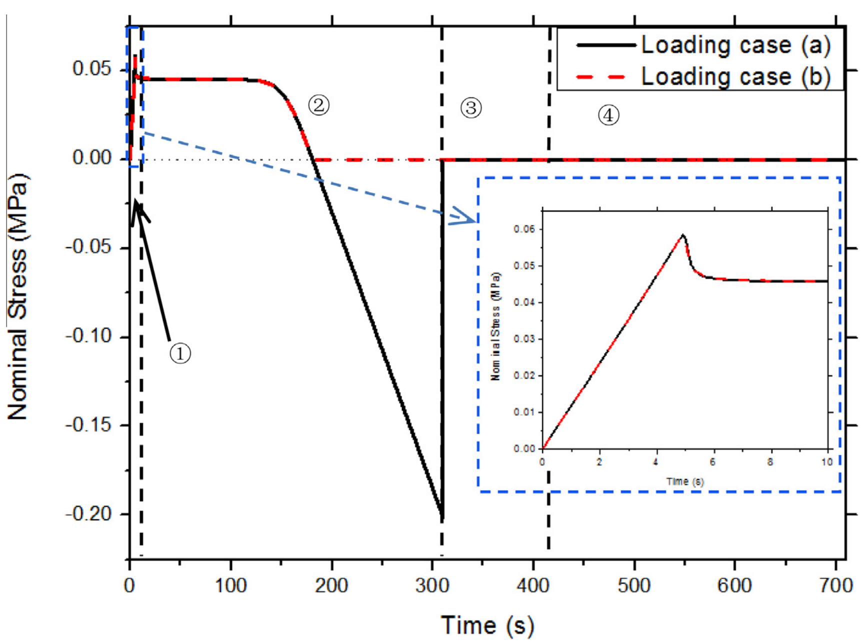

Fig. 6. Nominal stress response as a function of time during the compression inducing pattern transformation included shape memory circle (①–④ represent the four steps in the shape memory circle, the zooming part is the nominal stress as a function of time during the loading step at high temperature 70 °C).

from the platen. Thus, no extra nominal strain recovery appears in the third step because no nominal stress exists at the end of the second step. In the fourth step, the deformation is also fully recovered during the reheating process.

The nominal stress and the nominal strain responses of the shape memory circles are illustrated in Figs. 6 and 7, in which ①–④ represent the four steps in the shape memory circles.

In order to validate the pattern transformation in general cellular structure, we adopted another kind of periodic cellular structure with hexagonal holes. The RVE model of the periodic cellular structure with hexagonal holes is a $40 \times 40 \times 2\ \mathrm{mm}^3$ plate sample (plain strain or plain stress cases), and the side lengths of the hexagonal holes are 4.77 mm which also gives a porosity of 0.59. The boundary conditions are the same as those of loading case (a) for the circle-hole periodic cellular structure. The patterns at different stages during the shape memory circle are shown in Fig. 8, and the nominal strain and nominal stress responses as a function of time are shown in Fig. 9. Since the mechanical properties of the hexagon-hole periodic cellular structure are similar with those of circle-hole one, we only present the numerical result of circle-hole case in the following.

As shown in Figs. 6 and 7, the mechanical behaviors of the SMP periodic cellular structures are the same during the compression process for the loading case of Fig. 5(a) and (b), and so all the simulation results in the following relate to the loading case of Fig. 5(a). This is because this loading case needs not consider the contact and can reduce the computing time. From our present study, we also find temperature and loading nominal strain rate greatly influence the pattern transformation of SMP periodic cellular structures; the influence on pattern transformation is described with the critical nominal strain which relates to pattern transformation.

To study the influence of temperature on pattern transformation, a constant nominal strain rate of 0.01/s is used. Since the nominal stress versus nominal strain behaviors are the same for the temperature range from 0 °C to 30 °C, the critical nominal strain is only present at temperatures above 30 °C, as shown in Fig. 10. It is observed that the maximum critical nominal strain occurs at a temperature of about 45 °C, which means that a much longer time will be needed to achieve pattern transformation at about 45 °C under the loading nominal strain rate of 0.01/s.

To further investigate the influence of loading speed, four nominal strain rates with 0.01/s, 0.005/s, 0.002/s and 0.001/s are adopted. The simulations are carried out using several sets of samples. Each set contains four samples corresponding to the four nominal strain rates respectively at the temperature range from 30 °C to 70 °C. The critical nominal strains at different nominal strain rates as a function of temperature from 30 °C to 70 °C are illustrated in Fig. 11. From Fig. 11, we can observe that as the nominal strain rate increases, the temperature corresponding to the maximum critical nominal strain increases.

To explain the simulation results in more detail, the time–temperature superposition principle is introduced to re-plot the curves in Fig. 11. The critical nominal strain as a function of nominal strain rate (logarithmic form) is illustrated in Fig. 12(a). The reference temperature is selected as T_{ref} = 50 °C and the horizontal shift factor values can be obtained using the WLF function. The horizontal axis values after shift can be figured out with the following equation,

$$\lg(\upsilon) = \lg(\upsilon_0) - \frac{C_1(T - T_{ref})}{C_2 + T - T_{ref}} \tag{13}$$

where $\lg(\upsilon)$ is the horizontal axis value after shift, υ_0 is the initial nominal strain rate adopted in the simulation, C_1 = 10.17 and C_2 = 47.35 °C are the WLF constants, and T_{ref} = 50 °C is the reference temperature.

After horizontal shift, we have the master curve of critical nominal strain as a function of nominal strain rate at T_{ref} = 50 °C as shown in Fig. 12(b). If the nominal strain rate is $10^{-0.8}/\mathrm{s} = 0.1587/\mathrm{s}$, the critical nominal strain should be 0.2365; this case corresponds to the case in which the nominal strain rate is 0.01/s at a temperature of 45 °C before horizontal shift, and we can learn that the critical nominal strain at 50 °C is between 0.07 and 0.17 in the giving range of nominal strain rates from Fig. 12(a). Thus, if the explanation is right, using the time–temperature equivalence principle, we could predict the mechanical behavior of a wider range of nominal strain rates. To validate the explanation, we carry out a simulation at a nominal strain rate of 0.1587/s and a temperature of 50 °C. The nominal stress versus

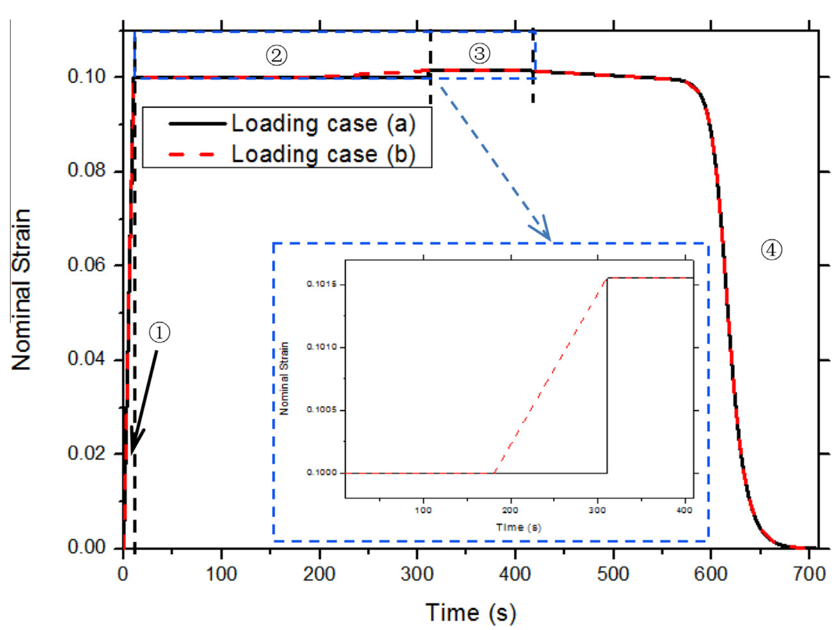

Fig. 7. Nominal strain response as a function of time during the compression inducing pattern transformation included shape memory circle (①–④ represent the four steps in the shape memory circle, the zooming part is the nominal strain as a function of time during the cooling and unloading steps).

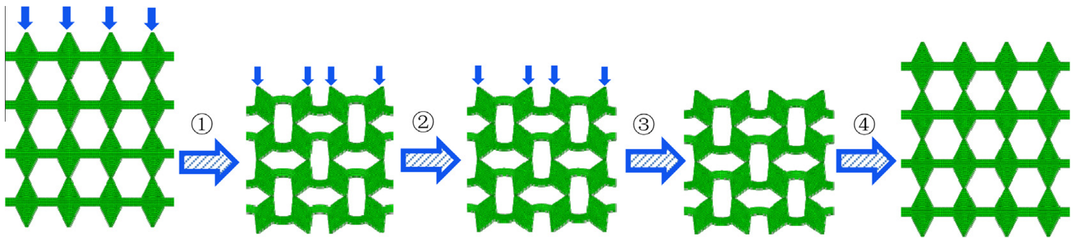

Fig. 8. Schematic plot of shape memory circle in hexagon-hole periodic cellular structures (①–④ represent the four steps in the shape memory circle).

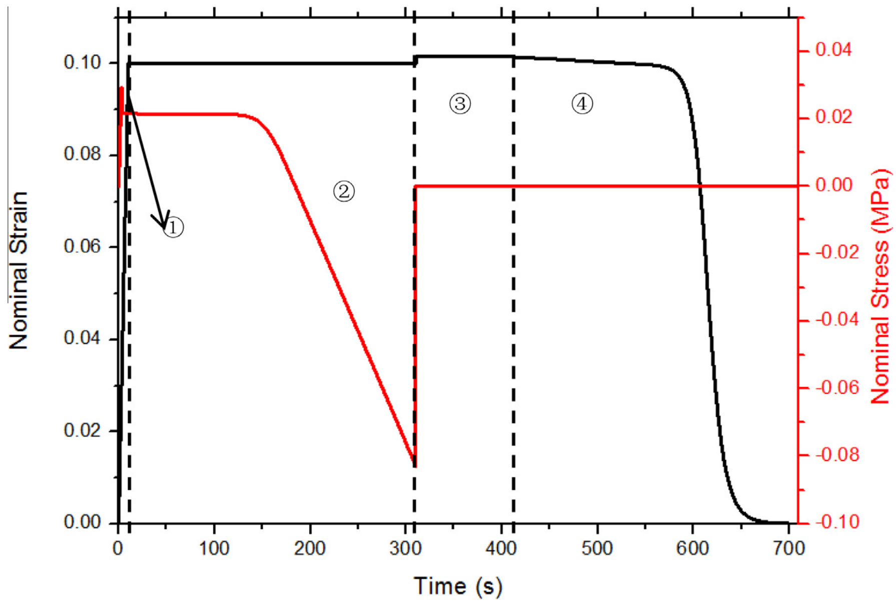

Fig. 9. Nominal strain and nominal stress response as a function of time during the compression inducing pattern transformation included shape memory circle in hexagon-hole periodic cellular structures (①–④ represent the four steps in the shape memory circle).

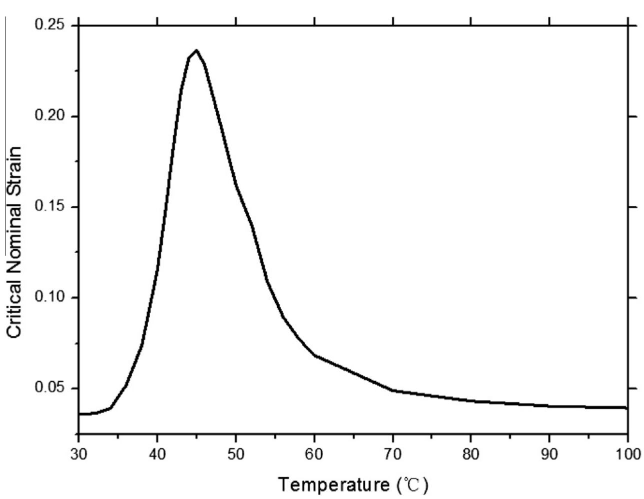

Fig. 10. Critical nominal strain as a function of temperature in the temperature range from 30 °C to 100 °C (the nominal strain rate is 0.01/s).

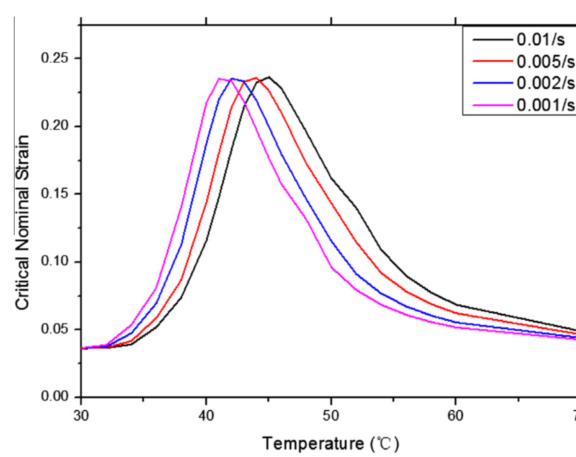

Fig. 11. Critical nominal strain as a function of temperature in the temperature range from 30 °C to 70 °C at different nominal strain rates.

nominal strain curves for different loading strain rates and temperatures are depicted in Fig. 13. From Fig. 13, it can be seen that the curve of nominal stress versus nominal strain behavior for nominal strain rate 0.1587/s at 50 °C (the black solid line) is identical to that of nominal strain rate 0.01/s at 45 °C (the red dash line), which means that the explanation is reasonable. These results are consistent with the time–temperature superposition principle and can serve as a cornerstone in transforming polymer behaviors between short-time ranges at high temperature and long-time ranges at low temperature.

3.2. Pattern transformation induced by stress relaxation

According to previous studies, it was typically understood that the pattern transformation of periodic cellular structures occurs

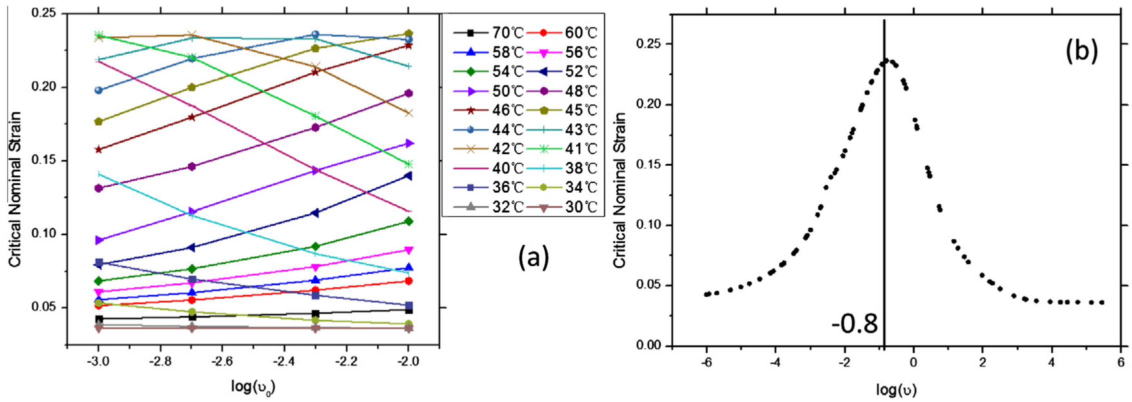

Fig. 12. (a) Critical nominal strain as a function of nominal strain rate at various temperatures. (b) Critical nominal strain versus nominal strain rate master curve obtained from horizontal shift of the data from (a); the reference temperature is 50 °C.

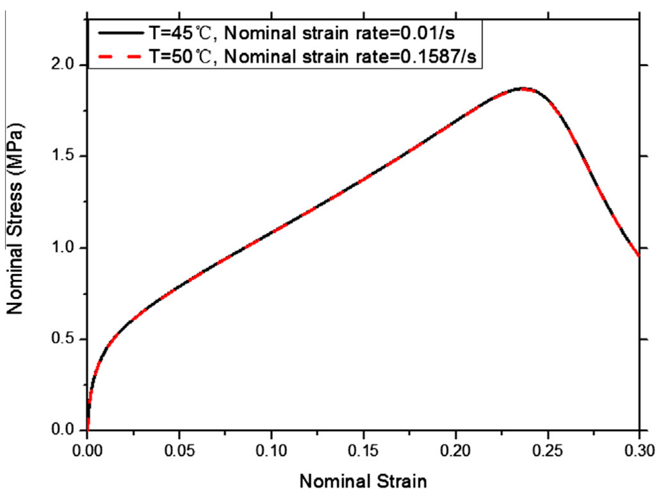

Fig. 13. Nominal stress versus nominal strain curves for nominal strain rate of 0.01/s at 45 °C and nominal strain rate of 0.1587/s at 50 °C.

only when the compressive nominal strain reaches a critical value. Nevertheless, from our extensive study of SMP materials, we find that the stress relaxation can also trigger pattern transformation, and that pattern transformation is reversible and repeatable. To study the shape memory behavior of pattern transformation induced by stress relaxation, the shape memory circle is designed, as shown in Fig. 14, which includes five steps. Step one is a loading step, in which the pattern transformation does not occur. In the loading, the compressive load is applied using the loading method shown in Fig. 5(a) to a nominal strain of 0.1 at a certain temperature and a nominal strain rate of 0.005/s. It should be noted that the critical nominal strain values of the present model are above 0.1 for temperatures in the range of 40 °C to 50 °C under a nominal strain rate of 0.005/s. This means that pattern transformation does not occur when the model is compressed in these conditions. Next is the relaxation step, in which pattern transformation appears. In step two, the temperature and nominal strain are kept the same as the values at the end of the first step for 300 s. Step three is the cooling step, in which the transformed pattern is fixed. In step three, we retain the nominal strain from the end of the second step and reduce the temperature to 0 °C in 210 s. Step four is the unloading step. Here, we remove the strain constraint in 1 s and maintain the low temperature state for another 99 s. Finally, we perform the reheating step, in which the transformed pattern is recovered. In step five, we raise the temperature to 70 °C in 300 s.

As shown in Fig. 15, for the hexagon-hole periodic cellular structure, the boundary conditions are the same as those of the circle-hole periodic cellular structure, and similar phenomena can be observed. Therefore, we will analyze only the mechanical properties of circle-hole periodic cellular structure in the following.

As mentioned above, for this kind of SMP material periodic cellular structure with a porosity of 0.59, the pattern transformation induced by stress relaxation after compressed to a nominal strain of 0.1 appears in the temperature range of 40 °C to 50 °C. Taking 50 °C as an example, the nominal stress and nominal strain responses during the shape memory circle are illustrated in Figs. 16 and 17 respectively.

From the nominal stress versus time curve shown in Fig. 16, we find that during the second step of shape memory cycle there are two stages, both of which contain two periods: a rapidly falling period and a slowly declining period. The intersection of the slowly declining period in the first stage and the rapidly falling period in the second stage is the pattern transformation critical point, which is marked with a solid dot in the plot. The nominal stress at this point is known as critical nominal stress. We can also say that the pattern transforms when the stress relaxes down to the critical nominal stress. In studying Fig. 17, it can be seen that there is no meaning for critical strain, as we retain the strain as a constant in step two. Therefore, we use critical stress to identify the pattern transformation critical point for the stress relaxation case.

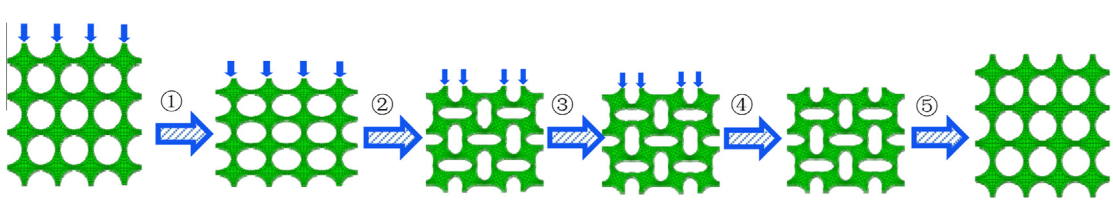

Fig. 14. Schematic diagram of relaxation inducing pattern transformation included shape memory circle for circle-hole case (①–⑤ represent the five steps in the shape memory circle respectively).

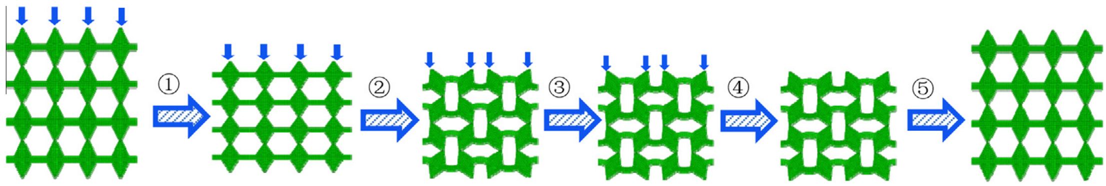

Fig. 15. Schematic diagram of relaxation inducing pattern transformation included shape memory circle for hexagonal-hole case (①–⑤ represent the five steps in the shape memory circle respectively).

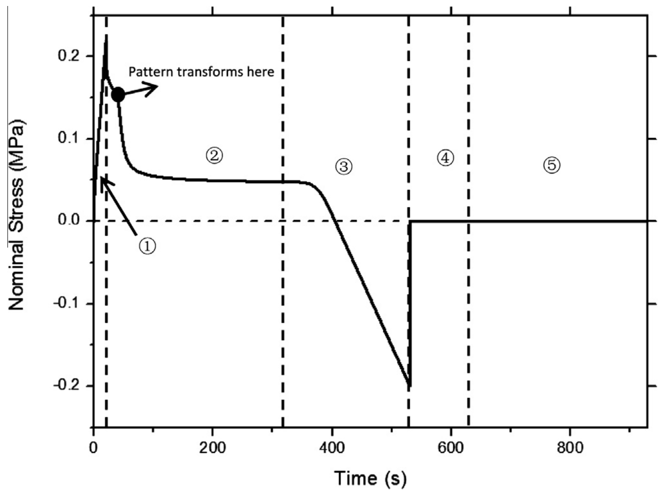

Fig. 16. Nominal stress response as a function of time during the relaxation which induces pattern transformation. The shape memory circle includes five steps which are depicted by step ①–step ⑤.

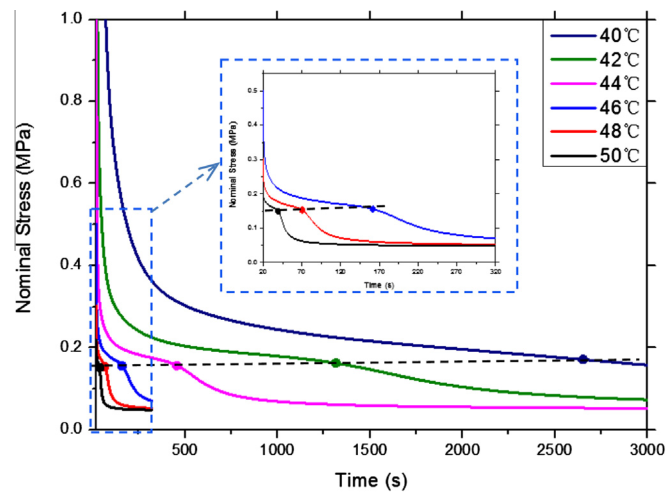

Fig. 18. Nominal stresses as a function of time during the relaxation step (relaxation time is 300 s for different temperatures above 45 °C and 3000 s for temperatures below 45 °C. The zooming part shows the nominal stress versus time curves for different temperatures above 45 °C).

To study the temperature influence on the pattern transformation induced by stress relaxation, we carry out simulations for every 2 °C increment in the temperature range of 40 °C to 50 °C. The simulations include two steps, the loading step and the relaxation step. These two steps are the same as the first two steps in the shape memory circle. The nominal stress versus time behavior curves during the relaxation step are illustrated in Fig. 18. From the curves, we can see that the pattern transformation occurs only when the nominal stress relaxes down to a critical value, and that the values show a minor discrepancy for different temperatures (the values of critical nominal stress become a little larger in the lower temperature range as the black dash lines show in Fig. 18). We also can observe that the higher the temperature is, the shorter time the pattern transformation needs, while the final nominal stresses tend to retain the same value after pattern transformation.

The auxetic (negative Poisson ratio) behavior of periodic cellular structures during uniaxial compression has been studied by Bertoldi et al. (2010) and Hu et al. (2013) for different non SMP materials. In the present study, we find that this auxetic behavior also appears in the pattern transformation that occurs during the stress relaxation process. The Poisson ratio versus time behavior

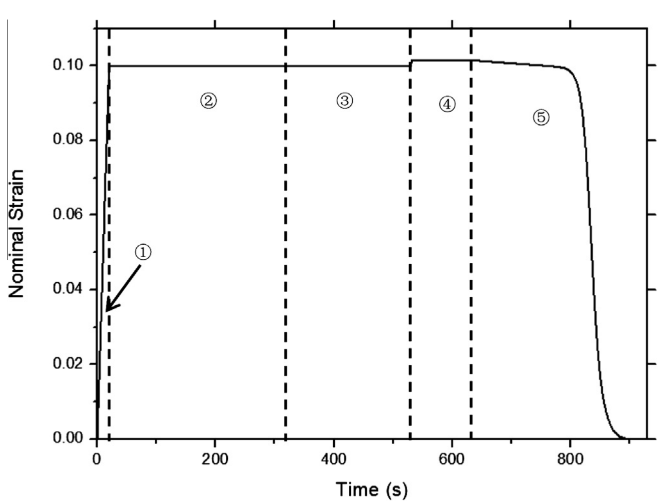

Fig. 17. Nominal strain response as a function of time during the relaxation which induces pattern transformation. The shape memory circle includes five steps which are depicted by step ①–step ⑤.

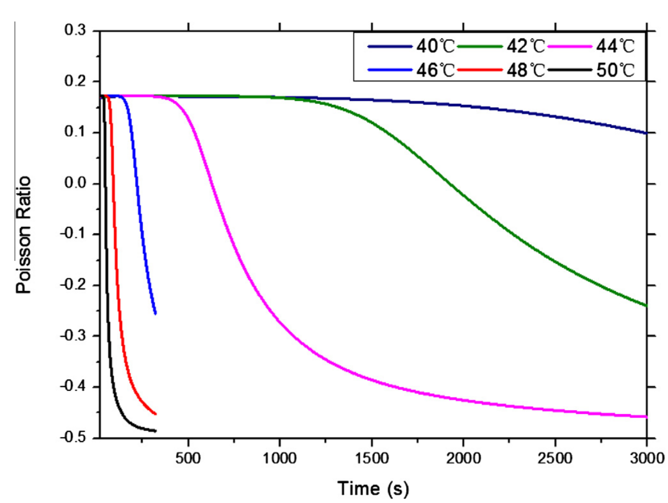

Fig. 19. Poisson ratio as a function of time during the relaxation step (the relaxation time is 300 s for temperatures above 45 °C and 3000 s for temperatures below 45 °C).

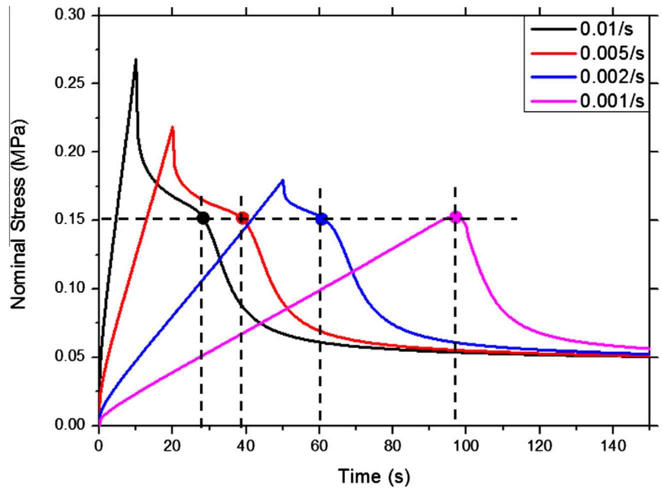

Fig. 20. Nominal stress as a function of time at 50 °C during the loading and relaxation steps (the loading nominal strain rate is different for each curve, but the nominal strains at the end of the loading step are at a same value of 0.1).

during the relaxation step for different temperatures in the range of 40 °C to 50 °C is illustrated in Fig. 19. From this figure, we can observe that the Poisson ratios begin to decrease after pattern transformation and become negative as time increases.

From this study, we find that different loading speeds can lead to different nominal stresses for the model at the same nominal strain, and different nominal stresses take different times to relax to the critical value for the pattern transformation. To study these effects, we carry out further simulations. In the following simulations, different nominal strain rates are chosen to apply to the samples at 50 °C during the loading step but the nominal strains at the end of the loading are taken as the same value of 0.1. The nominal stress versus time behavior curves are shown in Fig. 20. In Fig. 20, the increasing periods of the curves represent the loading steps and the declining periods represent the relaxation steps.

From Fig. 20, it can be found that the maximum nominal stress is higher for a faster loading speed at the end of the loading step, and the time taken for the maximum stress to relax to the critical value is longer. However, the total time taken for the occurrence of pattern transformation is shorter for a faster loading speed. Therefore, from these results it can be drawn that we could take advantage of this phenomenon (rapid loading and relaxation) to alter the time taken for pattern transformation.

Since the stress relaxation would speed up if we raise the temperature, the pattern transformation should also speed up if the temperature is raised. To further study the influence of temperature, we carry out the following simulations. First, the samples are compressed to a nominal strain of 0.1 at 46 °C and all nominal strain rates are taken as 0.01/s. Then, the samples are relaxed at different temperature conditions, i.e., the constant temperature relaxation (the temperature is kept constant at 46 °C during the relaxation process), the gradually rising temperature relaxation (the temperature is increased gradually from 46 °C to 60 °C) and the high temperature relaxation (the temperature is altered to 60 °C at the beginning of the relaxation step and is maintained at 60 °C during relaxation). The nominal stress history as a function of time during the relaxation step is shown in Fig. 21(a). For the constant temperature relaxation case (the black line), the nominal stress gradually decreases to the critical nominal stress at about 150 s, which means that the pattern transformation takes place at about 150 s; for the gradually rising temperature relaxation case (the red line), the nominal stress gradually decreases to the critical nominal stress at about 60 s, which means that the pattern transformation occurs at about 60 s; and for the high temperature relaxation case (the blue line), the nominal stress suddenly declines to the critical nominal stress, which means that the pattern suddenly transforms at the beginning of relaxation. The patterns of the samples for the three relaxation cases at the different times of 25 s, 100 s and 200 s are shown in Fig. 21(b).

4. Concluding remarks

To describe SMP's intrinsic viscoelasticity and time–temperature dependent behavior, we employ the generalized Maxwell model and the WLF equation to perform pattern transformation simulations. Simulations are carried out on the SMP periodic cellular structures. This type of structure can display an interesting phenomenon of novel pattern transformation when compressed beyond a critical value or when in a stress relaxation process. The pattern transformation is triggered by elastic instability and thus is reversible and repeatable. For SMP materials, the transformed pattern can be fixed in a cooling process to a temperature

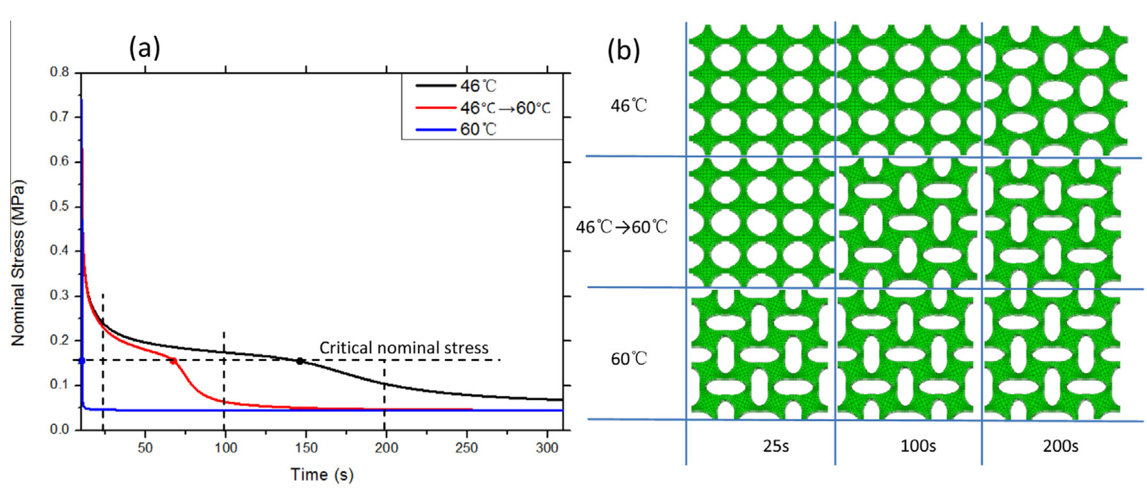

Fig. 21. (a) Nominal stress as a function of time during the relaxation step. (b) Deformed pattern for three different relaxation cases. The loading step is the same where the sample is compressed to a nominal strain of 0.1 at 46 °C in 10 s, while the relaxation steps are different and are illustrated with lines in different colors. The black line represents a temperature during relaxation of 46 °C, the red line represents the temperature during relaxation changing gradually from 46 °C to 60 °C, the blue line represents the temperature changing to 60 °C at the beginning of the relaxation step and maintaining 60 °C during relaxation. The values of time axis shows the total time which includes the loading step and relaxation step. (For interpretation of the references to color in this figure legend, the reader is referred to the web version of this article.)

below T_g and the fixed pattern can recover to the initial pattern when reheating to a temperature above T_g. Nominal strain rate and temperature can influence the pattern transformation process. The effects of nominal strain rate and temperature on the pattern transformation process are investigated through finite element simulation approaches, and we provide a physical explanation using the time–temperature superposition principle. The study shows the possibility of predicting the unknown pattern transformation mechanical behaviors of SMP periodic cellular structures in various loading conditions with known pattern transformation mechanical behavior in certain loading condition, and thus can reduce experimental costs. The study also presents a method for obtaining a mechanical behavior that is unable to realize with the usual method. We could take advantage of the fact that the mechanical behaviors obey the time–temperature equivalence principle to design suitable experimental and manufacturing processes. Although the simulation is based on epoxy network SMPs, similar phenomena should be observable for other viscoelastic materials with time–temperature dependent properties. This work indicates the exciting prospect of a technological advance by imprinting complex patterns during fabrication processes using a minimum number of developmental steps and time, and would inspire people interested in experiments about the technological advance. We hope this study can contribute to the research on pattern transformation of SMP periodic cellular structures, and predict their mechanical behaviors in various loading conditions.

Acknowledgments

The authors are grateful for the support from the National Natural Science Foundation of China through grant numbers 11372236, 11321062 and 51378448. The work described in this paper was also supported by grants from the Research Grants Council of the Hong Kong Special Administrative Region, China (Project No. 9042047, CityU 11208914).

Appendix A

The implementation of the mechanical behavior in ABAQUS input file are listed as below.

```
*Material, name = Polym
*Expansion
5.7e−05,50.
2.44e−06,55.
*Hyperelastic, neo hooke, moduli = INSTANTANEOUS
393.964, 0.0006452
*Viscoelastic, time = PRONY
0.187327        0.,     3.031e−05
0.222863        0.,     0.0001721
0.257003        0.,     0.0009768
0.225274        0.,     0.005545
0.0863276       0.,     0.03147
0.0144556       0.,     0.1787
0.00287336      0.,     1.014
0.00103207      0.,     5.757
0.000510199     0.,     32.68
0.000223371     0.,     185.5
6.41683e−05     0.,     1053.
1.60548e−05     0.,     5977.
*Trs
50., 10.17, 47.35
```

References

Abaqus/Standard, 2011. Dassault Systems Simulia Corporation, Providence, RI, USA.
Abrahamson, E.R., Lake, M.S., Munshi, N.A., Gall, K., 2003. Shape memory mechanics of an elastic memory composite resin. J. Intell. Mater. Syst. Struct. 14, 623–632.
Arrieta, J.S., Diani, J., Gilormini, P., 2014a. Experimental and modelling studies of the shape memory properties of amorphous polymer network composites. Smart Mater. Struct. 23, 639–650.
Arrieta, S., Diani, J., Gilormini, P., 2014b. Experimental characterization and thermoviscoelastic modeling of strain and stress recoveries of an amorphous polymer network. Mech. Mater. 68, 95–103.
Baghani, M., Naghdabadi, R., Arghavani, J., 2013. A large deformation framework for shape memory polymers: constitutive modeling and finite element implementation. J. Intell. Mater. Syst. Struct. 24, 21–32.
Behl, M., Kratz, K., Noechel, U., Sauter, T., Lendlein, A., 2013. Temperature-memory polymer actuators. Proc. Nat. Acad. Sci. USA 110, 12555–12559.
Bertoldi, K., Boyce, M.C., 2008. Mechanically triggered transformations of phononic band gaps in periodic elastomeric structures. Phys. Rev. B 77, 052105.
Bertoldi, K., Reis, P.M., Willshaw, S., Mullin, T., 2010. Negative Poisson's ratio behavior induced by an elastic instability. Adv. Mater. 22, 361–366.
Bhattacharyya, A., Tobushi, H., 2000. Analysis of the isothermal mechanical response of a shape memory polymer rheological model. Polym. Eng. Sci. 40, 2498–2510.
Chen, Y.-C., Lagoudas, D.C., 2008a. A constitutive theory for shape memory polymers. Part I. J. Mech. Phys. Solids 56, 1752–1765.
Chen, Y.-C., Lagoudas, D.C., 2008b. A constitutive theory for shape memory polymers. Part II. J. Mech. Phys. Solids 56, 1766–1778.
Diani, J., Gall, K., 2007. Molecular dynamics simulations of the shape-memory behaviour of polyisoprene. Smart Mater. Struct. 16, 1575–1583.
Diani, J., Frédy, C., Gilormini, P., Merckel, Y., Régnier, G., Rousseau, I., 2011. A torsion test for the study of the large deformation recovery of shape memory polymers. Polym. Testing 30, 335–341.
Diani, J., Gilormini, P., Frédy, C., Rousseau, I., 2012. Predicting thermal shape memory of crosslinked polymer networks from linear viscoelasticity. Int. J. Solids Struct. 49, 793–799.
Hu, J., He, Y., Lei, J., Liu, Z., 2013. Novel mechanical behavior of periodic structure with the pattern transformation. Theor. Appl. Mech. Lett. 3, 8–054007.
Hu, J., He, Y., Lei, J., Liu, Z., Swaddiwudhipong, S., 2014. Mechanical behavior of composite gel periodic structures with the pattern transformation. Struct. Eng. Mech. 50, 605–616.
Lendlein, A., Kelch, S., 2002. Shape-memory polymers. Angew. Chem. Int. Ed. 41, 2034–2057.
Lendlein, A., Jiang, H., Jünger, O., Langer, R., 2005. Light-induced shape-memory polymers. Nature 434, 879–882.
Lin, J., Chen, L., 1999. Shape-memorized crosslinked ester-type polyurethane and its mechanical viscoelastic model. J. Appl. Polym. Sci. 73, 1305–1319.
Liu, Y., Gall, K., Dunn, M.L., McCluskey, P., 2004. Thermomechanics of shape memory polymer nanocomposites. Mech. Mater. 36, 929–940.
Liu, Y., Gall, K., Dunn, M.L., Greenberg, A.R., Diani, J., 2006. Thermomechanics of shape memory polymers: uniaxial experiments and constitutive modeling. Int. J. Plast. 22, 279–313.
Liu, C., Qin, H., Mather, P.T., 2007. Review of progress in shape-memory polymers. J. Mater. Chem. 17, 1543.
Mather, P.T., Luo, X., Rousseau, I.A., 2009. Shape memory polymer research. Annu. Rev. Mater. Res. 39, 445–471.
Michel, J.C., Lopez-Pamies, O., Castaneda, P.P., Triantafyllidis, N., 2007. Microscopic and macroscopic instabilities in finitely strained porous elastomers. J. Mech. Phys. Solids 55, 900–938.
Morshedian, J., Khonakdar, H.A., Rasouli, S., 2005. Modeling of shape memory induction and recovery in heat-shrinkable polymers. Macromol. Theory Simul. 14, 428–434.
Mullin, T., Deschanel, S., Bertoldi, K., Boyce, M.C., 2007. Pattern transformation triggered by deformation. Phys. Rev. Lett. 99, 084301.
Mullin, T., Willshaw, S., Box, F., 2013. Pattern switching in soft cellular solids under compression. Soft Matter 9, 4951–4955.
Nguyen, T., Qi, H.J., Castro, F., Long, K., 2008. A thermoviscoelastic model for amorphous shape memory polymers: incorporating structural and stress relaxation. J. Mech. Phys. Solids 56, 2792–2814.
Nguyen, T.D., Yakacki, C.M., Brahmbhatt, P.D., Chambers, M.L., 2010. Modeling the relaxation mechanisms of amorphous shape memory polymers. Adv. Mater. 22, 3411–3423.
Prum, R.O., Quinn, T., Torres, R.H., 2006. Anatomically diverse butterfly scales all produce structural colours by coherent scattering. J. Exp. Biol. 209, 748–765.
Qi, H.J., Nguyen, T.D., Castro, F., Yakacki, C.M., Shandas, R., 2008. Finite deformation thermo-mechanical behavior of thermally induced shape memory polymers. J. Mech. Phys. Solids 56, 1730–1751.
Qiao, T., Liu, L., Liu, Y., Leng, J., 2013. Post buckling analysis of the shape memory polymer composite laminate bonded with alloy film. Compos. B Eng. 53, 218–225.
Simo, J.C., 1987. On a fully three-dimensional finite-strain viscoelastic damage model: formulation and computational aspects. Comput. Methods Appl. Mech. Eng. 60, 153–173.
Tobushi, H., Hara, H., Yamada, E., Hayashi, S., 1996. Thermomechanical properties in a thin film of shape memory polymer of polyurethane series. In: 1996

Symposium on Smart Structures and Materials. International Society for Optics and Photonics, pp. 46–57.
Tobushi, H., Hashimoto, T., Hayashi, S., Yamada, E., 1997. Thermomechanical constitutive modeling in shape memory polymer of polyurethane series. J. Intell. Mater. Syst. Struct. 8, 711–718.
Tobushi, H., Okumura, K., Hayashi, S., Ito, N., 2001. Thermomechanical constitutive model of shape memory polymer. Mech. Mater. 33, 545–554.
Vukusic, P., Sambles, J.R., 2003. Photonic structures in biology. Nature 424, 852–855.
Willshaw, S., Mullin, T., 2012. Pattern switching in two and three-dimensional soft solids. Soft Matter 8, 1747–1750.
Xu, W., Li, G., 2010. Constitutive modeling of shape memory polymer based self-healing syntactic foam. Int. J. Solids Struct. 47, 1306–1316.
Yakacki, C.M., Shandas, R., Lanning, C., Rech, B., Eckstein, A., Gall, K., 2007. Unconstrained recovery characterization of shape-memory polymer networks for cardiovascular applications. Biomaterials 28, 2255–2263.